Journal of Geophysical Research: Solid Earth

RESEARCH ARTICLE
10.1029/2017JB015108

Key Points:
- We propose a new hybrid model based on the ETAS model and Coulomb stress information
- We test this model on the 1992 Landers earthquake sequence
- We show an improvement of the results using this hybrid model compared to the classical ETAS model

Supporting Information:
- Supporting Information S1

Correspondence to:
T. Reverso,
thomas.reverso@adelaide.edu.au

Citation:
Reverso, T., Steacy, S., & Marsan, D. (2018). A hybrid ETAS-Coulomb approach to forecast spatiotemporal aftershock rates. *Journal of Geophysical Research: Solid Earth*, *123*, 9750–9763. https://doi.org/10.1029/2017JB015108

Received 12 OCT 2017
Accepted 12 OCT 2018
Accepted article online 17 OCT 2018
Published online 8 NOV 2018

A Hybrid ETAS-Coulomb Approach to Forecast Spatiotemporal Aftershock Rates

T. Reverso[1], S. Steacy[1], and D. Marsan[2]

[1]School of Physical Sciences, The University of Adelaide, Adelaide, South Australia, Australia, [2]ISTerre, Université de Savoie, Le Bourget du Lac, France

Abstract Aftershock sequences are an ideal testing ground for operational earthquake forecasting models as they contain relatively large numbers of earthquakes clustered in time and space. To date, most successful forecast models have been statistical, building on empirical observations of aftershock decay with time and earthquake size frequency distributions. Another approach is to include Coulomb stress changes from the mainshock which influence the spatial location of the aftershocks although these models have generally not performed as well as the statistical ones. Here we develop a new hybrid Epidemic-Type Aftershock Sequence (ETAS)/Coulomb model which attempts to overcome the limitations of its predecessors by redistributing forecast rate from negatively to positively stressed regions based on observations in the model learning period of the percentage of events occurring in those positively stressed regions. We test this model against the 1992 Landers aftershock sequence using three different ETAS kernels and five different models for slip in the Landers earthquake. We also consider two variations of rate redistribution, one based on a fixed value and the other variable depending on the percentage of aftershocks observed in positively stressed Coulomb regions during the learning period. We find that the latter model performs at least as well as ETAS on its own in all tests and better than ETAS in 14 of 15 tests in which we forecast successive 24-hr periods. Our results suggest that including Coulomb stress changes can improve operational earthquake forecasting models.

1. Introduction

In recent years, there has been a strong interest in developing operational earthquake forecasting models. The motivation and definition are described in Jordan et al. (2011), the basic idea is that "Operational earthquake forecasting is the dissemination of authoritative information about time-dependent probabilities to help communities prepare for potentially destructive earthquakes" (Jordan et al., 2014). In New Zealand, earthquake forecasts for both aftershocks and larger events are now routinely made available to the public (https://www.geonet.org.nz/earthquake/forecast/).

There are two main approaches to operational earthquake forecasting, physical and statistical. Physical models are generally based on the recognition that stress changes from earthquakes affect the timing and location of subsequent events (e.g., Steacy, Gomberg, & Cocco, 2005). Calculations of these so-called Coulomb stress changes can be combined with a rate state formulation for earthquake friction (Dieterich, 1994) to compute future earthquake rates. One limitation of these models is that the magnitude of the stress changes highly influences the aftershock occurrence rates (Dieterich, 1994), yet this in turn depends strongly on uncertain earthquake slip models (Hainzl et al., 2009).

The second main approach is based on statistical models which use different scaling laws that describe the mean features of earthquake sequences through empirical relations as the Omori-Utsu law (Utsu, 1961) and/or the magnitude frequency relation (Gutenberg & Richter, 1944). The most commonly used models are ETAS (*Epidemic-Type Aftershock Sequence*; e.g., Ogata, 1988, 1998) and STEP (*Short-Term Earthquake Probabilities*; e.g., Gerstenberger et al. (2005) which use these relations to estimate the seismicity rate.

These statistical models produce much different patterns of forecast earthquake rate than Coulomb-based ones because the spatial distribution of aftershocks is calculated with homogeneous spatial kernel functions. In contrast, Coulomb stress perturbation maps are quite heterogeneous.

A retrospective test of a number of different forecasting models was conducted by Woessner et al. (2011) for the Landers earthquake sequence. They compared the forecasting skill of two STEP models (with one

considered as the *reference model* for the entire suite), six ETAS ones, and four variations of Coulomb rate state. They found that ETAS models performed best overall and that the Coulomb models tended to be worse. The exception was a Coulomb-based model that incorporated significant stochasticity in the finite fault model.

Recently, a few authors have attempted to develop hybrid models which combine the spatial controls from the physical Coulomb model with the statistical information (Bach & Hainzl, 2012; Steacy et al., 2014) to forecast aftershock rates. For example, Bach and Hainzl (2012) developed a hybrid model which combined the ETAS model with a number of different elements, including static Coulomb stress changes. In the latter, the aftershock number was proportional to the magnitude of the Coulomb stress change in regions where this quantity was positive. They found that the addition of the static stress changes led to a better fit with more distant aftershocks. In their approach, the number of events was directly proportional to the Coulomb stress magnitude and hence the forecast number of events was very sensitive to the slip model used to estimate the static stress.

Steacy et al. (2014) applied a different method to the Canterbury earthquake sequence combining the STEP model (Gerstenberger et al., 2005) with Coulomb stress changes. In their approach, the Coulomb stress map was treated as a Boolean and 93% of forecast rate was redistributed from negatively stressed areas to positively stressed ones, based on observations from Southern California. They found that the combined STEP/Coulomb models could perform better than STEP on its own, but the results depended strongly on the slip models for the complex ruptures in the sequence.

Here we investigate a new hybrid model in which we combine Coulomb stress changes with a classical ETAS model to forecast aftershock rates following the 1992 M_w = 7.3 Landers earthquake. Following Steacy et al. (2014), we do not consider the magnitude of the stress change in estimating aftershock rates but we do consider both a fixed redistribution parameter (93%) and a variable one. We also test a number of different ETAS spatial kernels, and we compute Coulomb stress changes for five different slip models.

2. Data

We focus on the Southern California region in a box between −118°E and −115.5°E and between 33.5°N and 35°N. We use the U.S. Geological Survey earthquake catalog from 1 January 1980 to 28 June 1992 to estimate the first set of ETAS parameters (α, p, c, and κ_0). Our forecast period begins from the M_w = 7.3 Landers earthquake on 28 June 1992 and continues for 188 days until the end of the year. We include shallow earthquakes (i.e., ≤20 km) with magnitudes $\geq m_c$ = 3.0. We observe 713 earthquakes in the study before the M_w = 7.3 Landers earthquake and 1,161 subsequently.

3. Method

We first develop a 1-day forecast method to estimate the spatiotemporal number of earthquakes taking place during a period T_{Fi} using the seismicity produced in a learning period T_L. After each day, a new forecast period T_{Fi+1} and a new learning period T_{L+1}, taking account of day T_{Fi} are estimated (see Figure S1 in the supporting information). Below we describe the method in detail.

3.1. Estimation of the Number of Aftershocks

We use the ETAS model (Ogata, 1988, 1998) to calculate the number of events for each time step. The seismicity rate $R(t)$ for a time t is described as the sum of two components:

$$R(t) = \mu + \nu(t). \tag{1}$$

The first component represents the background seismicity rate $\mu(t)$, and the second $\nu(t)$ is the interaction term between earthquakes or events with magnitude higher than the completeness magnitude m_c. More precisely, the interaction term can be write as

$$\nu(t) = \sum_{i \mid t_i < t} \frac{\kappa_0 e^{(M_i - m_c)}}{(t + c - t_i)^p}, \tag{2}$$

where α, p, c, and κ_0 represent the ETAS parameters which characterize the statistical seismicity of the studied region. These ETAS parameters are estimated using the Expectation Maximization algorithm (see supporting information for more details), and they are recalculated after each day.

Using this triggering term, the expected number of direct aftershocks (or first generation) $N^1_{j(t_1,t_2)}$ produced by a mainshock j from a period t_1 to t_2 is

$$N^1_{j(t_1,t_2)} = \int_{t_1}^{t_2} \nu_j(t)\mathrm{d}t = \int_{t_1}^{t_2} \frac{\kappa_0 e^{(M_j - m_c)}}{(t + c - t_j)^p}\, \mathrm{d}t, \tag{3}$$

and the total number of direct aftershocks due to past earthquakes k between t_1 and t_2 is

$$N^1_{Af(t_1,t_2)} = \sum_{k \mid t_k \le t_1} N^1_{k(t_1,t_2)}. \tag{4a}$$

To calculate higher generation aftershocks $\left(\left\{N^{\varepsilon}_{Af(t_1,t_2)}, \varepsilon = 1,\ 2,\ 3, \ldots, z\right\}\right.$, with ε and z the index of generation and the final generation of aftershocks, respectively), we create 1,000 Monte Carlo simulations of forecasts. These simulations are made for every day of forecast, and we estimate the final number of events $N_{Af(t_1,t_2)}$ as a mean value for all generations and all simulations as follows:

$$N_{Af(t_1,t_2)} = \frac{1}{1000} \sum_{M=1}^{1000} \sum_{\varepsilon=1}^{z} N^{\varepsilon}_{Af(t_1,t_2)}. \tag{4b}$$

We use the value $N_{Af(t_1,t_2)}$ to evaluate the number of events for the day beginning at t_1 to t_2 using the historical seismicity to the day t_1.

We note that the number of earthquakes due to background seismicity is low in this study (μ(t) = 0.0494 Earthquakes/day). Consequently, we decide to neglect it because we focus on a short period of time (i.e., 188 days) and the number of events produced by this term is low (8 events for the entire study).

3.2. Earthquake Spatial Density

Here, we calculate the number of events in space using 3 different spatial kernel functions. We define firstly the earthquake spatial density $\Omega(x, y, t_1, t_2)$ for a period (t_1, t_2) as

$$\Omega(x, y, t_1, t_2) = \sum_{k \mid t_k < t_1} \left(N_{k(t_1,t_2)} \times f(r_k, m_k) \right), \tag{5}$$

where $r_k = \sqrt{(x - x_k)^2 + (y - y_k)^2}$ and $f(r, m)$ is the spatial kernel function based on the epicentral distance r and the magnitude m. To evaluate and compare the number of events in space, the study area is subdivided into n bins of 0.025° × 0.025°. The number of events per bin Nb^n_{for} for a period (t_1, t_2) is calculated as

$$Nb^n_{for} = \int_{x_1^n}^{x_2^n} \int_{y_1^n}^{y_2^n} \Omega(x, y, t_1, t_2)\mathrm{d}x\ \mathrm{d}y, \tag{6}$$

where x_1^n, x_2^n, y_1^n, and y_2^n are the edges of bin n. This method is applied for all earthquakes of our study period (including the Landers earthquake), and we generate three initial models (one for each spatial kernel) that do not take into account the static stresses generated by the Landers earthquake.

The spatial kernels $f(r, m)$, given here as areal density, depend on of the epicentral distance r and the magnitude m of the earthquake. We use the rupture length $L(m) = L_c \times 10^{0.5(m - m_c)}$ where L_c is the rupture length for an earthquake of magnitude m_c (L_c = 0.5 km for magnitude m_c = 3.0 in the following), consistent with the dislocation model (Eshelby, 1957) and observations showing constant stress drops for earthquakes (Kanamori & Anderson, 1975). The first spatial kernel is a power law function introduced by Ogata (1998) and classically used in spatiotemporal ETAS model,

$$f_{pl}(r,m) = \frac{(\gamma-1)\times L(m)^{\gamma-1}}{2\pi\left(r^2+L(m)^2\right)^{\frac{\gamma+1}{2}}}, \tag{7}$$

where γ is a constant characterizing the far-field decrease; models based on this kernel are referred to below as *Ogata*. The second (*Gaussian*) is given by

$$f_{gs}(r,m) = \frac{1}{2\pi L(m)^2}\, e^{\left(\frac{-r^2}{2L(m)^2}\right)}, \tag{8}$$

and the third one (*Moradpour*) was developed by Moradpour et al. (2014) to explain the behavior of aftershock density in California with three different regimes,

$$f_{mpl}(r,m) = \begin{cases} \alpha_m \dfrac{q r^{\theta-1} L(m)^q}{2\pi\left(r^{\theta+1}+L(m)^{\theta+1}\right)^{1+\frac{q}{\theta+1}}} \text{ if } r < R_c, \\ \beta_m \dfrac{d r^{\theta-1} L(m)^d}{2\pi\left(r^{\theta+1}+L(m)^{\theta+1}\right)^{1+\frac{d}{\theta+1}}} \text{ if } r > R_c,. \end{cases} \tag{9}$$

where R_c represents a critical distance equal to the schizosphere thickness, independent of the mainshock, and where the decay exponent d for $r > L(m)$ is larger than the previous one (i.e., q). In equation (7), we impose $\gamma = 2$ to satisfy the far-field aftershock distribution after a static stress change (Hill & Prejean, 2007), and in equation (9), α_m and β_m are normalizing constants. Also, we use the values $\theta = 0.6$, $q = 0.35$, $d = 1.2$, and $R_c = 10$ km as determined by Moradpour et al. (2014) for the Southern California seismic catalog.

In this study, the majority of earthquakes are modeled as point sources (at their epicenters here) and the spatial kernels corresponding to these events are calculated from those sources. The exceptions are the largest events of the sequence, Landers and Big Bear, where the spatial kernels are calculated from their fault ruptures rather than their epicenters as some ETAS parameters (especially α) can be underestimated if large earthquakes ruptures are not included in the ETAS model (Hainzl et al., 2008).

Different authors have tried various approaches to characterize this rupture extension. Ogata (1998) proposed that mainshock location corresponds to the centroid of the ellipsoid described by these aftershock locations. However, in this case the mainshock location is still a point source, although he replaced the distance decay r^2 in the spatial kernel by a specific function to maintain the effect of the ellipsoid aftershock locations.

Another approach is to keep the isotropic kernel but to calculate the distance between the aftershock location and shortest distance to the rupture instead of the distance between aftershock and epicenter (Bach & Hainzl, 2012; Marsan & Lengliné, 2010), whereas Guo et al. (2015) discretized the rupture zone and allowed each segment to trigger aftershock isotropically and independently.

In Marsan and Lengliné (2008), the authors showed that the size of mainshock affects the aftershock density function, and in both the Guo et al. (2015) and Bach and Hainzl (2012) studies, the size of patch surfaces or rupture length (respectively) scales with the empirical law given by Wells and Coppersmith (1994). Here we propose another method to estimate the spatial kernel due to the Landers and Big Bear earthquakes.

To implement this modification but keep the same decay law as the point source approach, we proceed as follows.

1. In general, only one rupture model is used for the fault trace (as for example the Wald and Heaton (1994), model for the Bach and Hainzl, 2012, paper). Here we compute a mean fault trace for the five different slip models presented in this paper.
2. We discretize this new fault trace as k source points (100 here), distributed homogenously, and we calculate the spatial kernel of these points.
3. Then, for each point $\{x, y\}$ of the study area, we keep the maximum value of the density spatial kernel produced by points along the fault trace
4. Finally, we divide these density values by a constant to keep the summation of all density values equal to 1.

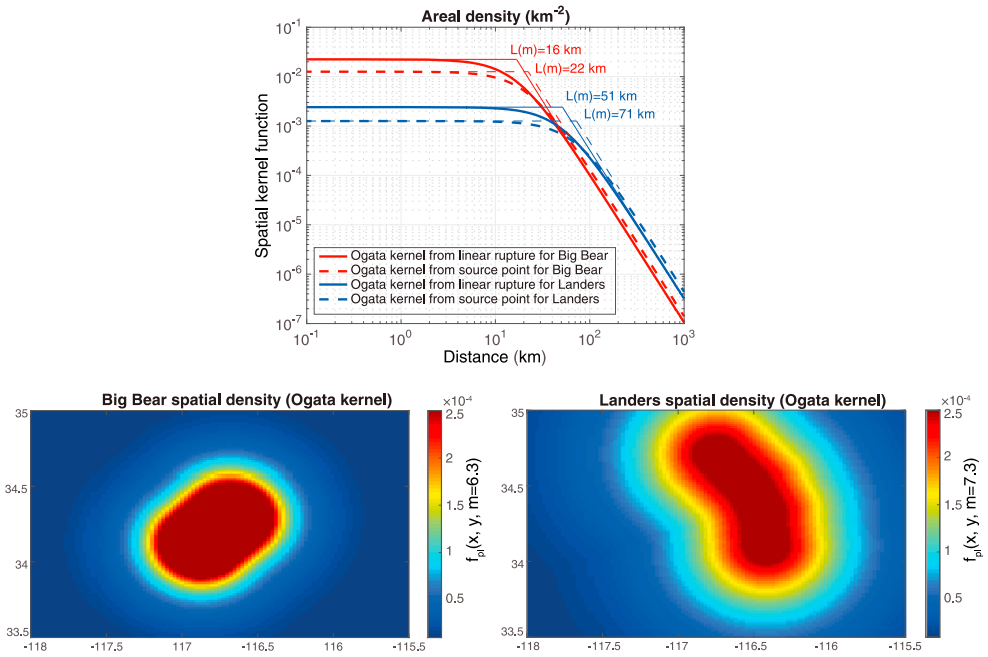

Figure 1. (top) Graph showing the Ogata spatial kernel function for the Landers (blue lines) and Big Bear earthquakes (red lines). The solid lines represent the spatial kernel from our study where the critical distance is optimized for a fault rupture, and the dashed lines represent the spatial kernel for a point source. (bottom) Specific spatial kernel for Big Bear (left) and Landers (right) used in this paper based on the Ogata kernel but modeled with the method explained in the text.

A critical point of this process is the value of rupture lengths $L_L(m)$ and $L_{BB}(m)$for Landers and Big Bear, respectively. The rupture length represents a characteristic value between two different parts of the spatial kernel (see Figure 1 for $L(m = 7.3)$). For example, in the Ogata spatial kernel, it separates a region where f_{pl} is constant between 0 to $L(m)$ and a second region where f_{pl} decreases as $r^{-\gamma-1}$.

However, with the process described above to calculate the Landers and Big Bear spatial kernel, this rupture length law produces an overly large region between 0 and $L(m)$. For example, if we keep the value of the L (m) = 71 km for the Landers earthquake, the area of region of constant f_{pl} between 0 and $L(m)$ will be much too large. In the far field both mainshocks are equivalent to point sources, and we can then simply use the spatial kernels described in equations (7) to (9). The lines of iso $f(x, y)$ are then circles, and the area with $f(x, y) < f(r = L(m))$ is that of a circle, hence with a surface $\pi \times L(m)^2$. In the near field, as the simulated spatial density becomes dependent on the complexity of the main fault, this approach yields a surface $f(x, y) < f(r = L(m))$ with an area much larger than $\pi \times L(m)^2$.

To resolve this problem, we calculate the area of a circle $A(r)$ defined by a radius $r = L(m)$ for each of the two Big Bear and Landers earthquakes. Then, we estimate new values of rupture length $L_L^{\text{rupt}}(m)$ and $L_{BB}^{\text{rupt}}(m)$ for Landers and Big Bear, respectively, using the following property

$$\mathscr{A}(L(m)) = \bigcup_{i=1}^{k} \mathscr{A}_i(L^{\text{rupt}}), \tag{10}$$

where $\mathscr{A}(L(m))$ is the circular area describe by the radius L and $\mathscr{A}_i(L^{\text{rupt}})$ is the circular area for the ith source point located on the fault rupture describe by the radius L^{rupt}. This method maintains the same area between 0 and $L(m)$ for the spatial kernel using a point source and for our spatial kernel used the finite fault trace (see Figure 1).

3.3. Redistribution With the Coulomb Stress Information

In a further two sets of models, we use Coulomb stress information as an additional filter to redistribute the number of events per bin. We use the program Farfalle (Nostro et al., 2002) to calculate the Coulomb stress

information for five different slip models of the Landers earthquake (i.e., Cohee & Beroza, 1994; Cotton & Campillo, 1995; Hernandez et al., 1999; Wald & Heaton, 1994 and Zeng & Anderson, 2000) which are available at http://equake-rc.info/SRCMOD/searchmodels/allevents/. We include the Big Bear earthquake in our stress modeling due to its proximity, magnitude, and occurrence time: 35 km west of Landers epicenter, $M_w = 6.3$, and approximately 3 hours after the Landers. We model it as a vertical failure of 23.3-km length located between 3- and 9-km depths with a left-lateral slip of 1.00 m (Murray et al., 1993) and for a strike orientation of ~N°45. Note that we do not include stress changes from smaller events because of the difficulties associated with modeling stress changes from smaller events including choice of the empirical relation for estimating the rupture dimensions and slip, location errors, difficulties in selecting the correct nodal plane, and lack of information about the location of the epicenter with respect to the rupture plane (Meier et al., 2014; Segou & Parsons, 2014; Steacy et al., 2014). For the aftershocks occurring between the time of the Landers and Big Bear earthquakes, we use only the Landers Coulomb stress map for the redistribution, and for earthquakes after Big Bear, the combined Coulomb stress map is used.

The Coulomb stress changes are computed on 2-D optimally oriented planes assuming right-lateral strike-slip target faults as Steacy, Nalbant, et al. (2005) showed that this was the best choice for the region of the Landers earthquake. The total stress tensor is defined as $\sigma^{tot} = \sigma^{r} + \sigma^{co}$. The σ^{co} is the coseismic stress perturbation which depends on the geometrical and slip information from slip models, and σ^{r} corresponds to the regional stress field. We assume a regional uniaxial compressional stress of 10 MPa oriented N7°E (King et al., 1994) and use an effective friction coefficient of 0.3 (Hainzl et al., 2009). We calculate the Coulomb stress change per bin for depths between 0 and 20 km (with a 1-km depth step) and then average over these depths to obtain the final value of Coulomb stress per bin.

In one set of models, we redistribute the forecast rate to so that 93% occurs in positive areas and 7% in negative areas. This ratio, called here the Coulomb Redistribution Parameter (CRP), resulted from observations of several California seismic sequences and was used in the STEP/Coulomb model described above (Steacy et al., 2014). In a second set of models, we compute the CRP in the model learning periods based on the correspondence between the Coulomb stress maps and the observed aftershocks in those periods (Figure 2). We redistribute the rate in each forecast period by calculating the percentage of events that are forecast to occur in positively versus negatively stressed areas and rescaling those rates so that the percentage matches the CRP.

Below, we test whether models based on fixed or variable CRPs better forecast the seismicity and how the forecasts from these hybrid models compare to those from the pure ETAS models with the different spatial kernels.

4. Statistical Tests

4.1. *N*-Test

To test how well the models forecast the number of events per day, we use the modified *N*-test, proposed by Zechar et al. (2010), which compares the forecast number of events with the observed number. The authors proposed two metrics:

$$\delta_1 = 1 - F(N_{obs} - 1|N_{Af}) \text{ and } \delta_2 = F(N_{obs}|N_{Af}), \tag{11}$$

where $F(x|\mu)$ is the right-continuous Poisson cumulative distribution with expectation μ evaluated at x and N_{obs} and N_{Af} are the observed and forecast numbers of events. A low value of δ_1 indicates an underestimated forecast number, and a low value of δ_2 indicates an overestimated forecast number.

We implement the cumulative *N*-test as the sum of the events calculated daily since the Landers earthquake. As this cumulative *N*-test can be strongly influenced by a large difference between the number of forecast and observed events, we also look at the daily *N*-test, which is independent in time.

4.2. Information Gain per Earthquake

An efficient and easy way to interpret test is the Information Gain per Earthquake (IGPE) proposed by Rhoades et al. (2011). This test provides a comparison between two models (A and B for example) by calculation of an information gain $I_N(A, B)$ according to the equation

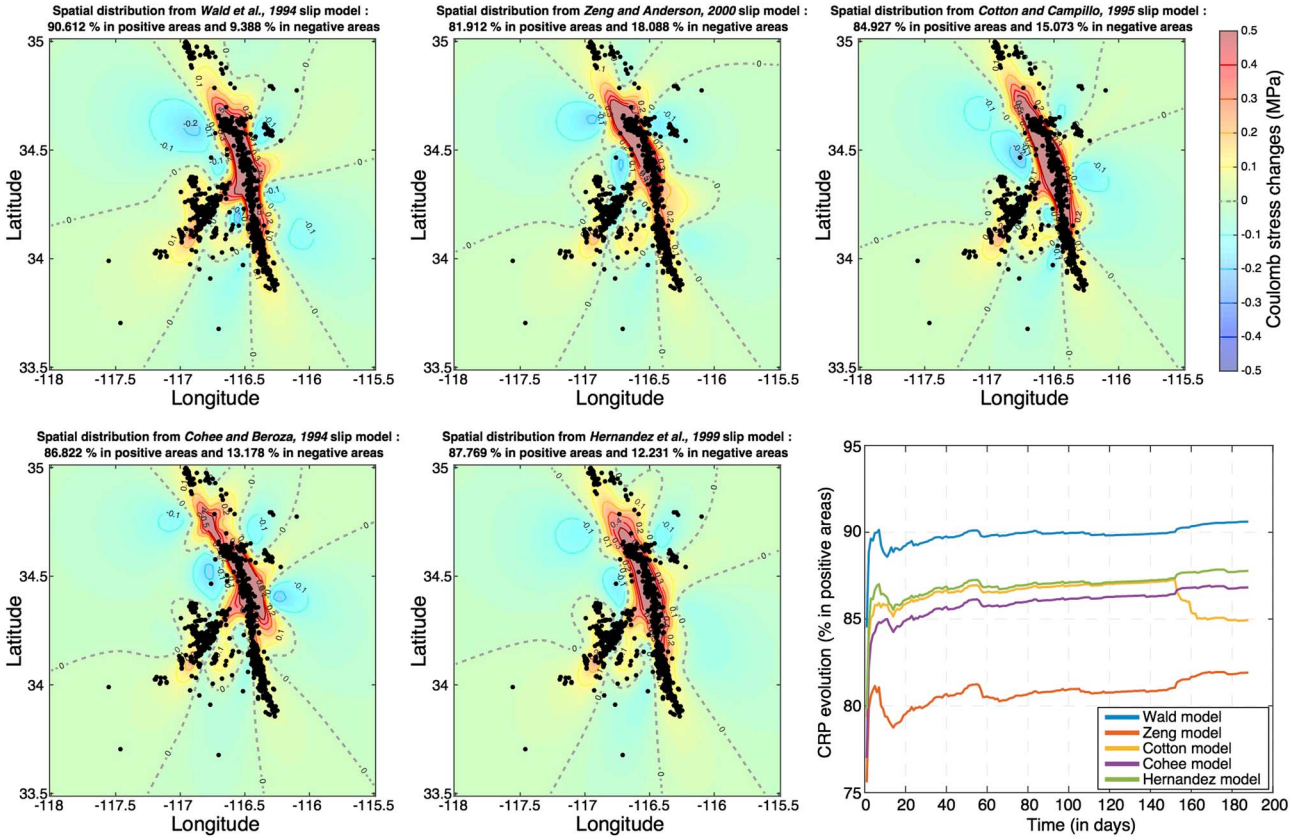

Figure 2. Spatial distribution of seismicity from different Coulomb stress maps at the end of the study. The five different Coulomb stress maps are calculated with different slip models (Cohee & Beroza, 1994; Cotton & Campillo, 1995; Hernandez et al., 1999; Wald & Heaton, 1994; Zeng & Anderson, 2000), and we represent the Coulomb stress map averaged over 0- to 20-km depth. Black dots correspond to the seismicity for the year 1992 between Julian day 179 (day 0) and year 1993 (day 188), and the gray dashed line is the limit between positive and negative Coulomb stress changes. The evolution of the CRP(t) in the positive areas and day after day is shown on the bottom right figure. CRP = Coulomb Redistribution Parameter.

$$I_N(A,B) = \frac{1}{N}\sum_{i=1}^{N} \ln\left(\frac{\lambda_A(k_i)}{\lambda_B(k_i)}\right) - \frac{\widehat{N}_A - \widehat{N}_B}{N}, \tag{12a}$$

where $\lambda_A(j)$ and $\lambda_B(j)$ are the number of events expected in models A and B, respectively, for a bin j; $\{k_i; i = 1, \ldots, N\}$ represents the bin where the earthquake i appeared; and $\widehat{N}_A$ (respectively, $\widehat{N}_B$) denotes the total number of earthquakes expected for model A (respectively, model B). The sample variance of $\ln\left(\frac{\lambda_A(k_i)}{\lambda_B(k_i)}\right)$ is given by

$$s^2 = \frac{1}{N-1}\sum_{i=1}^{N}\left(\ln\left(\frac{\lambda_A(k_i)}{\lambda_B(k_i)}\right)\right)^2 - \frac{1}{N^2-N}\left(\sum_{i=1}^{N}\ln\left(\frac{\lambda_A(k_i)}{\lambda_B(k_i)}\right)\right)^2, \tag{12b}$$

Thus, the final result with confidence intervals of the IGPE is

$$I(A,B) = I_N(A,B) \pm \frac{ts}{\sqrt{N}}, \tag{12c}$$

with t as the quantile of the t_{N-1} distribution. Below we show results with a 95% confidence interval. If that confidence interval does not cross the zero line, it indicates a significant difference in the information value of the two models.

4.3. Parimutuel Gambling Score

Nevertheless, the information gain test can be very sensitive to events occurring in low probability bins (Holliday et al., 2005). Hence, here we implement the parimutuel gambling scores (PGSs) developed by

Zechar and Zhuang (2014) that use the probability of each prediction per bin. In this test, each model is relatively compared and the test has the advantage that it limits the value of one bin (between −1 and 1), whereas the *R*-test and *T*-test can have an unbounded value for one bin.

In this test, the bins of our study are games, and each model proposes a different outcome for these games (see Zechar & Zhuang, 2014, for a detailed description of the method). For example, we could take the case of two forecast models Λ_j and Λ_R (indexes *j* and *R* refer to the *j*th forecast model and reference model, respectively), with respective probabilities p_j and p_R to have an event in one bin. This event can be the occurrence of one or several earthquakes or the occurrence of zero earthquake in the bin.

The test calculates a quantity, called *gambling return* Δr, as follows:

$$\Delta r_j = -1 + 2\frac{p_j}{p_j + p_R} \text{ and } \Delta r_R = -1 + 2\frac{p_R}{p_j + p_R}. \tag{13}$$

If the event occurs,

$$\Delta r_j = -1 + 2\frac{(1-p_j)}{(1-p_j)+(1-p_R)} \text{ and } \Delta r_R = -1 + 2\frac{(1-p_R)}{(1-p_j)+(1-p_R)} \tag{14}$$

if the event does not occur. For all *n* bins, the gambling return is calculated as follows:

$$\Delta R_j = \sum_{i=1}^{n} \Delta r_j^i. \tag{15}$$

This final quantity ΔR_j represents the total gambling return (or net return) for all bins of the *j*th forecast model. This test allows an efficient test to compare all models generated in this work. However, to aid the interpretation of our results, below we consider a pairwise model comparison between models.

5. Results

In this section, we describe the results for a series of 24-hr tests in which we optimize the ETAS parameters (i.e., α, *p*, *c*, and κ_0) after each day in order to forecast the seismicity for the next 24 hr. Note that the learning periods are cumulative in that a 24-hr forecast for any given day is based on the ETAS parameters computed over the entire preceding catalog. The first set corresponds to the ETAS parameter estimation from 1 January 1980 to the day of the Landers earthquake (day 0); the second set includes the seismicity on day 0; the third the seismicity on day 1, etc. The evolution of these parameters is shown in Figure 3 where we observe a significant change after the estimation of the first set of parameters. As the Landers earthquake is the largest earthquake in the study area since 1980, its aftershock sequence strongly disrupts the regional seismicity estimation. After this day, the ETAS parameters follow a quite regular evolution which is likely due to missing aftershocks after the Landers earthquake.

This effect is tested in the supporting information (Figure S2). We compare the evolution of the ETAS parameters for a complete synthetic catalog including an aftershock sequence after an M = 7.3 earthquake and the same catalog where we removed aftershocks after a mainshock M = 7.3 using the completeness magnitude equation $m_c(t) = M - 4.5 - 0.32 \times \log(t)$ from Helmstetter et al. (2006). In this example, we observe a similar pattern for α and κ_0 to what we observe following the Landers earthquake and also a more complex evolution for parameters *p* and *c* which are strongly perturbed by missing events.

In the first step of our forecasting approach, we calculate the number of events for each day *d* using the historical seismicity from the 1992 M_w = 7.3 Landers earthquake to the day $(d - 1)$ (see Figure S1).

The forecast and observed number of events are shown in Figure 4 where we observe that the values are broadly similar. The first day of the forecast has the greatest difference between the forecast and observed number of events (267.5 and 310 events, respectively) which can be explained by a lack of earthquakes between magnitude m_c and magnitude M = 4.0 (Woessner et al., 2011) due to an increase of the magnitude of completeness immediately following the Landers earthquake. Another reason is a consequence of ETAS

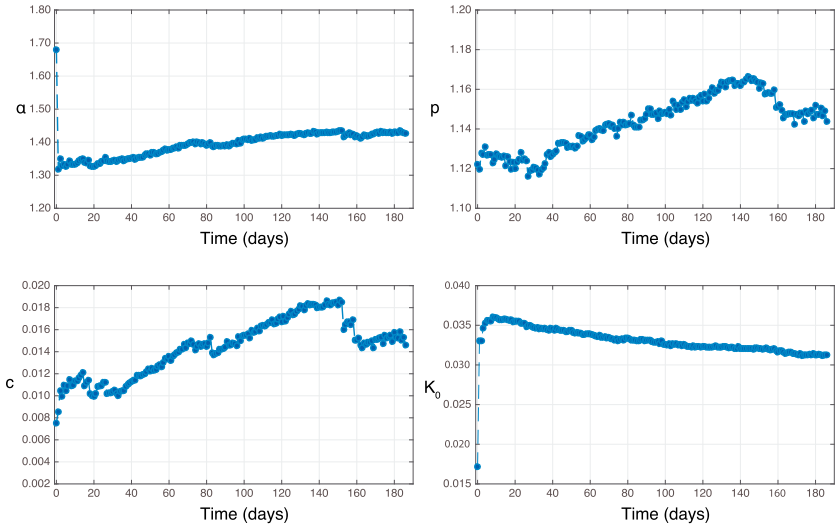

Figure 3. Evolution of Epidemic-Type Aftershock Sequence parameters. These estimations are calculated from 1 January 1980 for earthquakes with magnitudes $\geq m_c$, and they are reestimated after each day of forecast period. We observe an important change after the first day due to the Landers/Big-Bear aftershock sequences.

parameters estimation: as the ETAS parameters represent the mean values for the historical seismicity, these parameters are maladjusted for the more unusual mainshock-aftershock sequences such as the uncommon M_w = 7.3 Landers earthquake and hence can produce an underestimate or overestimate of the expected number of events. In this case the number of events is underestimated.

To address the issue with the magnitude of completeness, we use the same approach as Woessner et al. (2011), and we estimate the number of events during the first day from $m_c >$ =4.0. We observe 62 events during this day, and we forecast for this day 32.9 events. To have this forecast, we use the Gutenberg Richter law with a *b* value of 0.91 (i.e., the same *b* value used by Woessner et al., 2011).

The results of the *N*-test for the forecast number of events per day are shown in Figure 4. We estimate the cumulative quantile scores δ_1 and δ_2 since day 1, to have an overall model performance with a memory of the daily performance (Figure 4). We introduce a significance level of 0.05 to reject the worst forecasts. The cumulative quantile scores δ_1 between days 1 and 69 are below the 0.05 significance level, showing that the forecast number of events is too high. However, this cumulative test is strongly influenced by the large difference between the observed and forecast numbers of events in the first 3 days where we forecast, respectively, 32.9, 69.9, and 48.1 events but 62, 103, and 93 are observed. If we calculate the daily fraction R_N (daily) of *N*-test where δ_1 or δ_2 are lower than the effective significance level

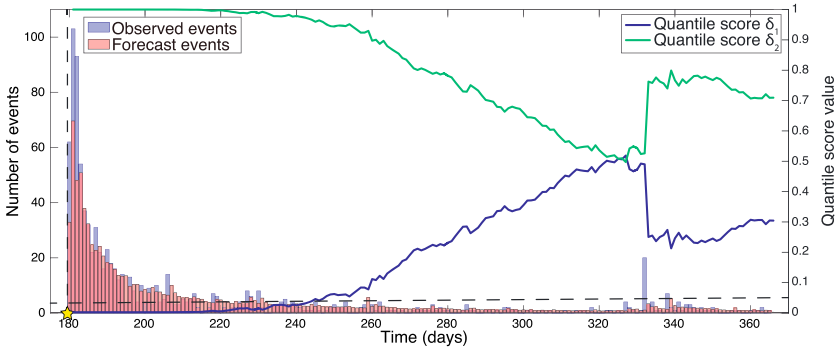

Figure 4. Observed and forecast number of events per day, superimposed on quantile scores for earthquakes with magnitude > = 3.0 beginning at day 180 (*t* = 1). The horizontal dashed gray line indicates the 0.05 significance level at which the test is rejected.

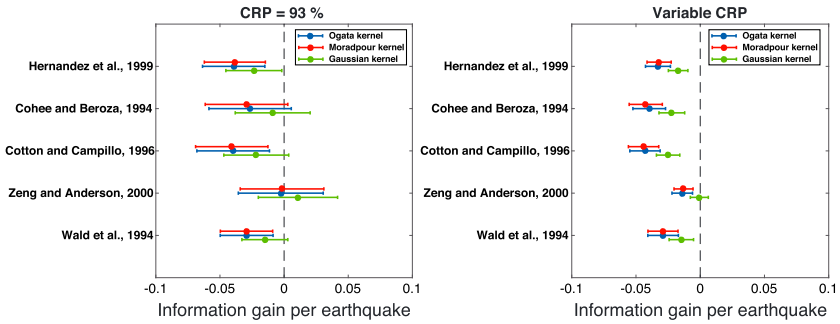

Figure 5. Results of the Information gain per Earthquake (IGPE) for the entire study using both a CRP of 93% and a variable CRP. The different colors indicate the spatial kernel used. Each plot shows the mean and 95% confidence interval of the IGPE, and a negative information gain implies that the hybrid model is better than the classical ETAS model. Finally, if the confidence interval does not intersect the zero value, the IGPE is significant. CRP = Coulomb Redistribution Parameter; ETAS = Epidemic-Type Aftershock Sequence.

α_{eff} = 0.025 (defined by Zechar et al., 2010), we find a value of R_N (daily) = 0.0699 (i.e., 13 forecasts over 186 are lower than α_{eff} and 3 of them during the first 3 days) showing that only 7% of our forecasts are inconsistent with observation.

The results for the IGPE are shown in Figure 5 for the entire study period. We observe that the Gaussian kernel is the most inconsistent one as it underpins the only set of models where our hybrid approach does not improve the classical ETAS model. We also observe that all hybrid models based on the Moradpour and Ogata spatial kernels and with a variable value of CRP are always significantly better than classical ETAS models. We note, however, that the information gains are quite small.

To test the spatial forecasts per bin, we calculate the total net return for a pairwise case and we estimate the PGS after each day; we show the cumulative number of the PGS(t) in Figures 6 and 7. In Figure 6, we compare only the ETAS models (i.e., without Coulomb stress information). Although the Moradpour kernel appears to outperform the Ogata one in Figure 6 (left), this is misleading because the result is dominated by the value (11.6) on day 1. This is shown by the continued decrease in the PGS(t) throughout the time period. For the same reason, the comparison between the Moradpour and Gaussian kernels in Figure 6 (right) does not really indicate which is the best one. However, as shown in Figure 6 (middle), the reference model (Gaussian kernel) performs worse than the Ogata kernel.

In Figure 7, we compare models using Coulomb stress information to their corresponding models without this information for both variable CRP (in red) and CRP = 93% (in blue). We observe that models based on variable CRP almost invariably perform better than reference models for the first month after the Landers mainshock. Models using CRP = 93% can perform worse than the reference model as showed for the Zeng case and Gaussian spatial kernel. This is consistent with the IGPE results (Figure 5) in which Zeng/Gaussian model with CRP = 93% performs no better than the corresponding ETAS model.

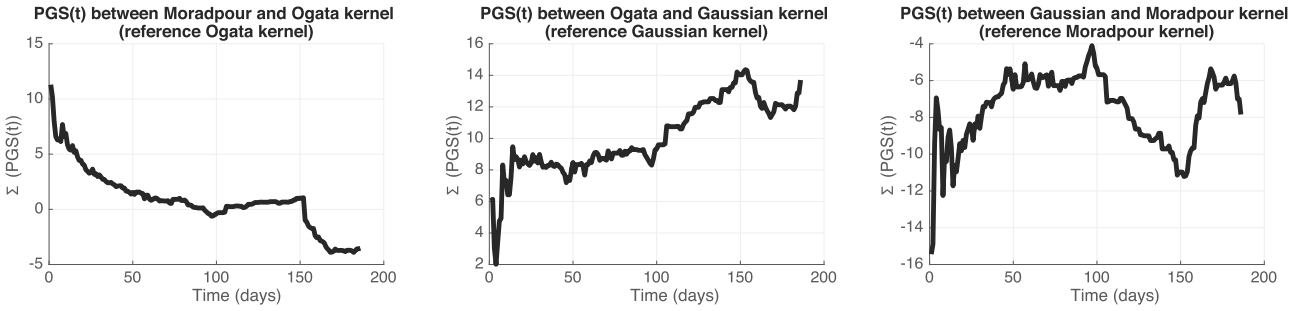

Figure 6. The cumulative Parimutuel Gambling Score (PGS) results for each model without Coulomb stress information, function of time t. If the cumulative PGS(t) value is negative, the reference model is the best model; otherwise, the other model is the best. PGS = Parimutuel Gambling Score.

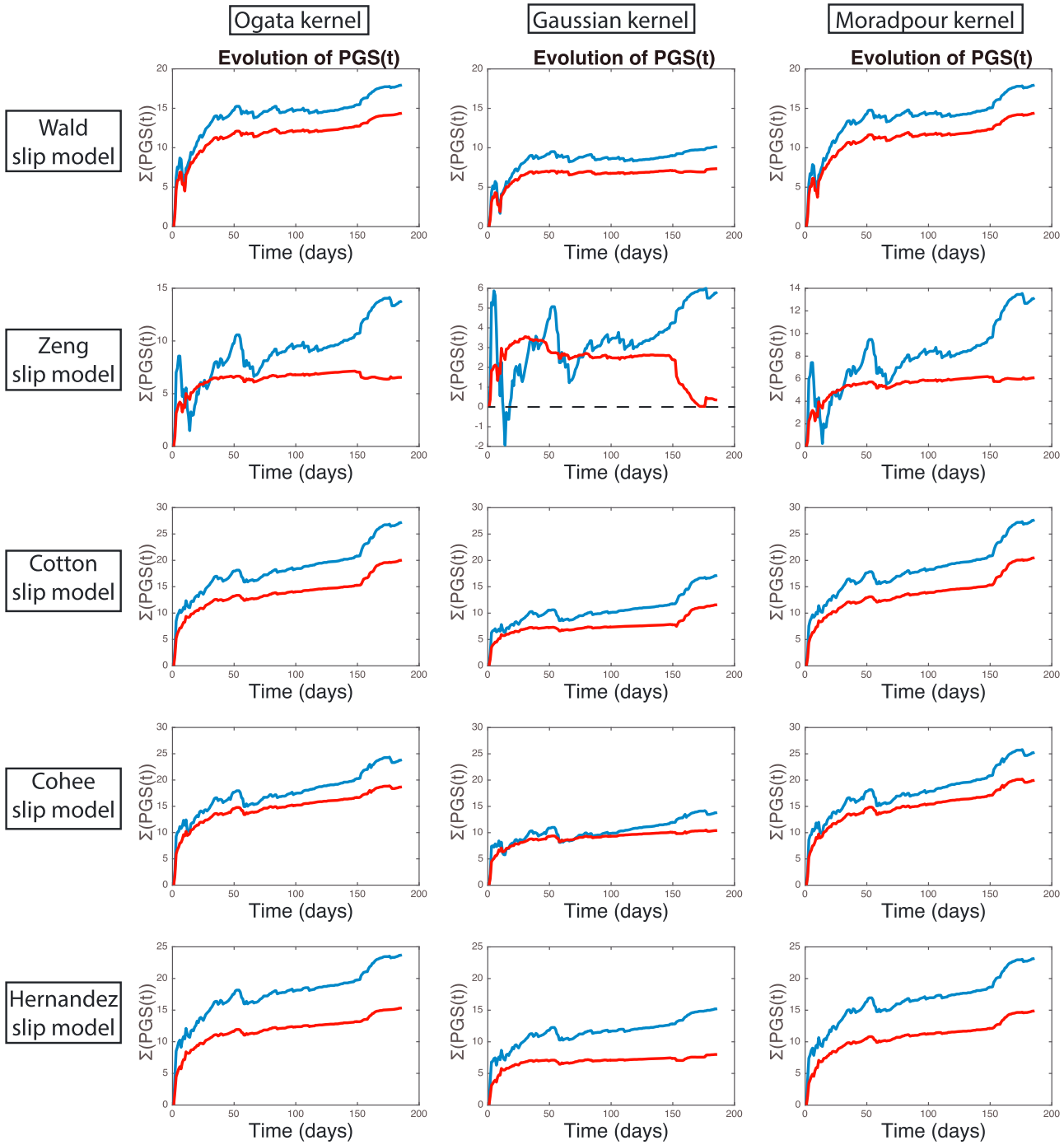

Figure 7. The cumulative Parimutuel Gambling Score (PGS) results for each model using Coulomb stress information compared to the model without Coulomb stress information. The solid blue line indicates the PGS for a constant CRP = 93% and in red the PGS result for models using an optimal CRP. The black dotted line for the value 0 indicates when the reference model is better (when value in negative) for the test.

6. Forecasts for 15, 30, 60, and 120 Days

In this section, we use the Ogata kernel to forecast the earthquake number and locations for forecast periods ending at 15, 30, 60, and 120 days after the Landers earthquake. We use three different learning periods: the first day following the earthquake, then the 5 days and finally the 10 days after it.

Table 1
Comparison of Observed (N_{obs}) and Forecast (N_{for}) Number of Events for Different Learning Periods and Forecast end Dates

		Number of events					
		1 day		5 days		10 days	
Last day of forecast period		N_{for}	N_{obs}	N_{for}	N_{obs}	N_{for}	N_{obs}
	15 days	281 ± 47	493	185 ± 38	206	74 ± 21	83
	30 days	370 ± 64	590	315 ± 63	303	213 ± 49	180
	60 days	474 ± 83	688	474 ± 90	401	372 ± 78	278
	120 days	590 ± 104	760	656 ± 119	473	555 ± 113	350

Note. The 1 day and 5 and 10 days refer to the length of the learning period.

We observe that our forecasts based on a 1-day learning period always underestimate the number of events (Table 1). A possible explanation is due to undetected earthquakes during the first day as the mainshock/aftershock sequences due to these earthquakes lack cannot be modeled by ETAS. Also, the misestimation of the ETAS parameters, specially an underestimation of the α parameter due to missing events after Landers occurrence (see Seif et al., 2017), could be a reason for this underestimation of events.

However, for longer learning periods (i.e., for 5 and 10 days), the number of events is quite consistent with observation for forecast periods 3 to 4 times longer than the learning period.

Finally, we forecast the earthquake rates in space and time for the same forecast periods using the Ogata kernel (the best spatial kernel in this study) and compare the results for ETAS on its own to the hybrid ETAS/Coulomb (vCRP) model. As Figure 8 illustrates, the hybrid model significantly outperforms ETAS on its own in 51 of 60 tests.

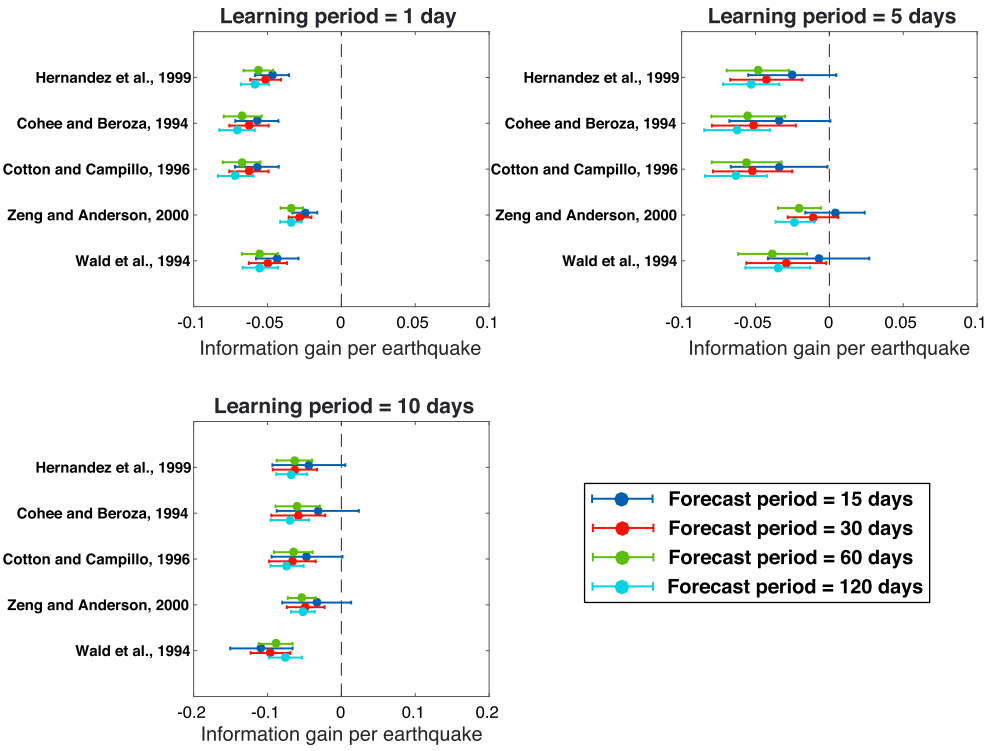

Figure 8. Results of Information gain per Earthquake (IGPE) for different learning periods, different forecasts, and different slip models. The different colors indicate the forecast period used for these hybrid models. Each plot shows the mean and 95% confidence interval of the IGPE, and a negative information gain implies that the hybrid model is better than the classical Epidemic-Type Aftershock Sequence model. Finally, if the confidence interval does not intersect the zero value, the IGPE is significant.

7. Discussion and Conclusions

Our most important result is that the hybrid ETAS/Coulomb model with a variable CRP almost invariably performs better than the ETAS model on its own. This is a much stronger result than the observations of Bach and Hainzl (2012) and Steacy et al. (2014) that hybrid Coulomb/statistical models performed better than statistical ones only in certain circumstances.

We believe that there are two reasons for this result. The first is that our approach only depends on the sign of the Coulomb stress change, not its spatially dependent magnitude. The latter is strongly dependent on the details of the earthquake slip distribution which cannot be uniquely determined (Hainzl et al., 2009). In addition, the generic CRP of 93% adopted by Steacy et al. (2014) overestimated the percentage of events occurring in positively stressed areas. In the Canterbury sequence they studied, for instance, about 76% of events following the Darfield earthquake took place in areas of positive Coulomb stress (Steacy et al., 2013), much less than the 93% assumed in their study.

The percentage of Landers aftershocks in positively stressed areas in our study varies from about 90% for the Wald slip model to approximately 80% for the Zeng model (Figure 2). As the former is close to our fixed CRP of 93%, it is not surprising that the PGSs for this slip model are very similar for the fixed and variable CRP models (Figure 7). In contrast, the fixed CRP model performs significantly worse than the variable one for the Zeng slip model.

The poor result for the fixed CRP model is consistent with the suggestion of Steacy et al. (2014) that the performance of their hybrid STEP/Coulomb model depended strongly on the quality of the slip distribution. However, allowing a variable CRP appears to compensate for this, as shown in Figure 7 where the hybrid ETAS/vCRP Coulomb model outperforms ETAS even for the worst performing slip model (Zeng).

Of the three ETAS kernels evaluated in this study, the Gaussian kernel consistently performs the worst. This is likely because it has the most rapid decrease in forecast numbers with distance (Figure 1), and hence, it underpredicts more distant aftershocks. Interestingly, the addition of the Coulomb filter dramatically improves the performance of the hybrid model based on the Gaussian kernel (Figure 7) because it pushes rate further from the fault zone in positively stressed regions. This is also true for the other kernels, but the effect is less pronounced because the kernels themselves distribute rate into those more distant areas.

Although most of our results are for 24-hr tests, we also forecast aftershocks over longer time periods. From a societal perspective, longer time period forecasts may be more useful for emergency response—for instance, in determining where to locate an emergency shelter. Unfortunately, the longer-term forecasts underpredict the number of aftershocks, although this decreases significantly with longer learning periods (Table 1) suggesting that these are more appropriate for longer-term forecasts than shorter learning periods.

Acknowledgments
We thank Max Werner, Shyam Nandan, and the Associate Editor for constructive comments which significantly improved the manuscript. We used the earthquake catalog provided by the Southern California Earthquake Data Center (SCEDC) and all the slip models used come from the Finite-source rupture model database, SRCMOD (http://equake-rc.info/SRCMOD/searchmodels/allevents/) initiated by M. P. Mai.

References

Bach, C., & Hainzl, S. (2012). Improving empirical aftershock modeling based on additional source information. *Journal of Geophysical Research*, *117*, B04312. https://doi.org/10.1029/2011JB008901

Cohee, B. P., & Beroza, G. C. (1994). Slip distribution of the 1992 Landers earthquake and its implications for earthquake source mechanics. *Bulletin of the Seismological Society of America*, *84*, 692–712.

Cotton, F., & Campillo, M. (1995). Frequency domain inversion of strong motions: Application to the 1992 Landers earthquake. *Journal of Geophysical Research*, *100*, 3961–3975. https://doi.org/10.1029/94JB02121

Dieterich, J. (1994). A constitutive law for rate of earthquake production and its application to earthquake clustering. *Journal of Geophysical Research*, *99*, 2601–2618. https://doi.org/10.1029/93JB02581

Eshelby, J. D. (1957). The determination of the elastic field of an ellipsoidal inclusion and related problems. *Proceedings of the Royal Society of London Series A*, *241*(1226), 376–396. https://doi.org/10.1098/rspa.1957.0133

Gerstenberger, M. C., Wiemer, S., Jones, L. M., & Reasenberg, P. A. (2005). Real-time forecasts of tomorrows earthquakes in California. *Nature*, *435*(7040), 328–331. https://doi.org/10.1038/nature03622

Guo, Y., Jiancang, Z., & Zhou, S. (2015). An improved space-time ETAS model for inverting the rupture geometry from seismicity triggering. *Journal of Geophysical Research: Solid Earth*, *120*, 3309–3323. https://doi.org/10.1002/2015JB011979

Gutenberg, B., & Richter, C. F. (1944). Frequency of earthquakes in California. *Bulletin of the Seismological Society of America*, *34*, 185–188.

Hainzl, S., Christophersen, A., & Enescu, B. (2008). Impact of earthquake rupture extensions on parameter estimations of point-process models. *Bulletin of the Seismological Society of America*, *98*, (4)2066–2066. https://doi.org/10.1785/0120070256

Hainzl, S., Enescu, B., Cocco, M., Woessner, J., Catalli, F., Wang, R., & Roth, F. (2009). Aftershock modeling based on uncertain stress calculations. *Journal of Geophysical Research*, *114*, B05309. https://doi.org/10.1029/2008JB006011

Helmstetter, A., Kagan, Y. Y., & Jackson, D. D. (2006). Comparison of short-term and time-independent earthquake forecast models for southern California. *Bulletin of the Seismological Society of America*, *96*(1), 90–106. https://doi.org/10.1785/0120050067

Hernandez, B., Cotton, F., & Campillo, M. (1999). Contribution of radar interferometry to a two-step inversion of the kinematic process of the 1992 landers earthquake. *Journal of Geophysical Research*, *104*, 13,083–13,099. https://doi.org/10.1029/1999JB900078

Hill, D., & Prejean, S. (2007). In G. Schubert (Ed.), *Dynamic triggering, chap. vol. 4: Earthquake seismology* (pp. 257–292). Amsterdam: Elsevier.

Holliday, J. R., Nanjo, K. Z., Tiampo, K. F., Rundle, J. B., & Turcotte, D. L. (2005). Earthquake forecasting and its verification. *Nonlinear Processes in Geophysics*, *12*(6), 965–977. https://doi.org/10.5194/npg-12-965-2005

Jordan, T., Chen, Y.-T., Gasparini, P., Madariaga, R., Main, I., Marzocchi, W., Papadopoulos, G., et al. (2011). Operational earthquake forecasting. State of knowledge and guidelines for utilization, final report of the international commission on earthquake forecasting for civil protection. *Annals of Geophysics*, *54*(4). https://doi.org/10.4401/ag-5350

Jordan, T. H., Marzocchi, W., Michael, A. J., & Gerstenberger, M. C. (2014). Operational earthquake forecasting can enhance earthquake preparedness. *Seismological Research Letters, Seismological Society of America (SSA)*, *85*(5), 955–959. https://doi.org/10.1785/0220140143

Kanamori, H., & Anderson, D. L. (1975). Theoretical basis of some empirical relations in seismology. *Bulletin of the Seismological Society of America*, *65*, 1073–1095.

King, G. C., Stein, R. S., & Lin, J. (1994). Static stress changes and the triggering of earthquakes. *Bulletin of the Seismological Society of America*, *84*, 935–953.

Marsan, D., & Lengliné, O. (2008). Extending earthquakes' reach through cascading. *Science*, *319*(5866), 1076–1079. https://doi.org/10.1126/science.1148783

Marsan, D., & Lengliné, O. (2010). A new estimation of the decay of aftershock density with distance to the mainshock. *Journal of Geophysical Research*, *115*, B09302. https://doi.org/10.1029/2009JB00711

Meier, M.-A., Werner, M. J., Woessner, J., & Wiemer, S. (2014). A search for evidence of secondary static stress triggering during the 1992 Mw 7.3 Landers, California, earthquake sequence. *Journal of Geophysical Research: Solid Earth*, *119*, 3354–3370. https://doi.org/10.1002/2013JB010385

Moradpour, J., Hainzl, S., & Davidsen, J. (2014). Nontrivial decay of aftershock density with distance in Southern California. *Journal of Geophysical Research: Solid Earth*, *119*, 5518–5535. https://doi.org/10.1002/2014JB010940

Murray, M. H., Savage, J. C., Lisowski, M., & Gross, W. K. (1993). Coseismic displacements: 1992 Landers, California, earthquake. *Geophysical Research Letters*, *20*, 623–626. https://doi.org/10.1029/93GL00446

Nostro, C., Baumont, D., Scotti, O., & Cocco, M. (2002), "Farfalle" Compute code: User's manual. Report of EC project "PRESAP" (towards practical, Real-time estimation of spatial aftershock probabilities: A feasibility study in earthquake hazard, EVK4–1999-00001), www.errigal.ulst.ac.uk/, University of Ulster, Coleraine Co. Derry., N. Ireland.

Ogata, Y. (1988). Statistical models for earthquake occurrences and residual analysis for point processes. *Journal of the American Statistical Association*, *83*(401), 9–27. https://doi.org/10.1080/01621459.1988.10478560

Ogata, Y. (1998). Space-time point-process models for earthquake occurrences. *Annals of the Institute of Statistical Mathematics*, *50*(2), 379–402. https://doi.org/10.1023/a:1003403601725

Rhoades, D., Schorlemmer, D., Gerstenberger, M., Christophersen, A., Zechar, J., & Imoto, M. (2011). Efficient testing of earthquake forecasting models. *Acta Geophysica*, *59*(4), 728–747. https://doi.org/10.2478/s11600-011-0013-5

Segou, M., & Parsons, T. (2014). The stress shadow problem in physics-based aftershock forecasting: Does incorporation of secondary stress changes help? *Geophysical Research Letters*, *41*, 3810–3817. https://doi.org/10.1002/2013GL058744

Seif, S., Mignan, A., Zechar, J. D., Werner, M. J., & Wiemer, S. (2017). Estimating ETAS: The effects of truncation, missing data, and model assumptions. *Journal of Geophysical Research: Solid Earth*, *122*, 449–469. https://doi.org/10.1002/2016JB012809

Steacy, S., Gerstenberger, M., Williams, C., Rhoades, D., & Christophersen, A. (2014). A new hybrid Coulomb/statistical model for forecasting aftershock rates. *Geophysical Journal International*, *196*(2), 918–923. https://doi.org/10.1093/gji/ggt404

Steacy, S., Gomberg, J., & Cocco, M. (2005). Introduction to special section: Stress transfer, earthquake triggering, and time-dependent seismic hazard. *Journal of Geophysical Research*, *110*, B05S01. https://doi.org/10.1029/2005JB003692

Steacy, S., Jimenez, A., & Holden, C. (2013). Stress triggering and the Canterbury earthquake sequence. *Geophysical Journal International*. https://doi.org/10.1093/gji/ggt3380

Steacy, S., Nalbant, S. S., McCloskey, J., Nostro, C., Scotti, O., & Baumont, D. (2005). Onto what planes should Coulomb stress perturbations be resolved? *Journal of Geophysical Research*, *110*, B05S15. https://doi.org/10.1029/2004JB003356

Utsu, T. (1961). A statistical study of the occurrence of aftershocks. *Geophysical Magazine*, *30*, 521–605.

Wald, D. J., & Heaton, T. H. (1994). Spatial and Temporal Distribution of Slip for the 1992 Landers, California, Earthquake. *Bulletin of the Seismological Society of America*, *84*, 668–691.

Wells, D. L., & Coppersmith, K. J. (1994). New empirical relationships among magnitude, rupture length, rupture width, rupture area, and surface displacement. *Bulletin of the Seismological Society of America*, *84*, 974–1002.

Woessner, J., Hainzl, S., Marzocchi, W., Werner, M. J., Lombardi, A. M., Catalli, F., Enescu, B., et al. (2011). A retrospective comparative forecast test on the 1992 Landers sequence. *Journal of Geophysical Research*, *116*, B05305. https://doi.org/10.1029/2010JB007846

Zechar, J. D., Gerstenberger, M., & Rhoades, D. (2010). Likelihood-based tests for evaluating space-rate-magnitude earthquake forecasts. *Bulletin of the Seismological Society of America*, *100*(3), 1184–1195. https://doi.org/10.1785/0120090192

Zechar, J. D., & Zhuang, J. (2014). A parimutuel gambling perspective to compare probabilistic seismicity forecasts. *Geophysical Journal International*, *199*(1), 60–68. https://doi.org/10.1093/gji/ggu137

Zeng, Y., & Anderson, J. (2000). Evaluation of numerical procedures for simulating near-fault long-period ground motions using Zeng method., Report 2000/01 to the PEER Utilities Program.